The EMBO Journal (2011) 30, 2490–2500 | © 2011 European Molecular Biology Organization | All Rights Reserved 0261-4189/11
www.embojournal.org

THE EMBO JOURNAL

Nogo-B receptor is necessary for cellular dolichol biosynthesis and protein *N*-glycosylation

Kenneth D Harrison[1], Eon Joo Park[1], Ningguo Gao[2], Andrew Kuo[1], Jeffrey S Rush[3], Charles J Waechter[3], Mark A Lehrman[2] and William C Sessa[1,*]

[1]Department of Pharmacology and Vascular Biology and Therapeutics Program, Yale University School of Medicine, New Haven, CT, USA, [2]Department of Pharmacology, University of Texas-Southwestern Medical Center, Dallas, TX, USA and [3]Department of Molecular and Cellular Biochemistry, University of Kentucky College of Medicine, Lexington, KY, USA

Dolichol monophosphate (Dol-P) functions as an obligate glycosyl carrier lipid in protein glycosylation reactions. Dol-P is synthesized by the successive condensation of isopentenyl diphosphate (IPP), with farnesyl diphosphate catalysed by a *cis*-isoprenyltransferase (*cis*-IPTase) activity. Despite the recognition of *cis*-IPTase activity 40 years ago and the molecular cloning of the human cDNA encoding the mammalian enzyme, the molecular machinery responsible for regulating this activity remains incompletely understood. Here, we identify Nogo-B receptor (NgBR) as an essential component of the Dol-P biosynthetic machinery. Loss of NgBR results in a robust deficit in *cis*-IPTase activity and Dol-P production, leading to diminished levels of dolichol-linked oligosaccharides and a broad reduction in protein *N*-glycosylation. NgBR interacts with the previously identified *cis*-IPTase hCIT, enhances hCIT protein stability, and promotes Dol-P production. Identification of NgBR as a component of the *cis*-IPTase machinery yields insights into the regulation of dolichol biosynthesis.

The EMBO Journal (2011) **30,** 2490–2500. doi:10.1038/emboj.2011.147; Published online 13 May 2011
Subject Categories: membranes & transport; cellular metabolism
Keywords: *cis*-IPTase; dolichol; *N*-glycosylation; protein

Introduction

Isoprenoids represent the most abundant and structurally diverse natural products known, consisting of >55 000 primary and secondary metabolites (Swiezewska and Danikiewicz, 2005). The carbon chain length of isoprenoids varies greatly, from the relatively short-chain geranyl diphosphate (C_{10}) to the long-chain structure of natural rubber ($C_{>10\,000}$). The mevalonate pathway is responsible for the generation of the numerous isoprenoids that are essential for cell viability. This pathway is characterized by a critical branchpoint intermediate, farnesyl pyrophosphate (FPP), which is generated by a *trans*-isoprenyltransferase (*trans*-IPTase) activity and serves as the basic building block for all subsequent steps in isoprenoid biosynthesis.

Three activities utilize FPP as a substrate to generate diverse lipids (Grunler *et al*, 1994). Squalene synthase is responsible for the first committed step towards the eventual production of cholesterol (Schroepfer, 1981, 1982), whereas two prenyltransferase activities function in the remaining pathways downstream of FPP, a *trans*-IPTase associated with production of the ubiquinone prenyl side chain via solanesyl and decaprenyl diphosphate synthesis (Teclebrhan *et al*, 1993) and a *cis*-isoprenyltransferase (*cis*-IPTase) involved in dolichol production (Gough and Hemming, 1970; Adair *et al*, 1984). Dolichol consists of 15–23 isoprene units (Rip *et al*, 1985; Schenk *et al*, 2001a) and is necessary for protein *N*-glycosylation and *O*-mannosylation, *C*-mannosylation of tryptophan, and GPI anchor biosynthesis.

The process of N-linked glycosylation is well characterized relative to our understanding of the synthesis of the glycosyl carrier lipid. Fourteen distinct lipid-linked oligosaccharide (LLO) intermediates are synthesized during the assembly of the final *N*-glycan donor molecule in the ER (Burda and Aebi, 1999). These steps in LLO biosynthesis take place on both sides of the ER bilayer, with the GlcNAc-1-phosphotransferase catalysing the first step on the cytosolic face of the ER by addition of a GlcNAc-1-P residue from a UDP-GlcNAc donor to dolichol monophosphate (Dol-P). The GlcNAc-P-P-Dol undergoes a series of further reactions at the cytoplasmic leaflet utilizing UDP-GlcNAc and GDP-Man until it is elongated to $Man_5GlcNAc_2$-P-P-Dol (M5-LLO). The LLO intermediates mannose-P-dolichol (Man-P-Dol) and glucose-P-dolichol (Glc-P-Dol) are also synthesized on the cytosolic leaflet of the ER, with GDP-Man and UDP-Glc serving as the respective glycosyl donors. Once synthesized, the M5-LLO, Man-P-Dol, and Glc-P-Dol intermediates are flipped in a protein-dependent manner to the luminal side of the ER, where the M5-LLO is elongated further through addition of four additional mannose units and three glucose residues until it reaches the mature state of $Glc_3Man_9GlcNAc_2$-P-P-Dol (G3M9-LLO). These sugars are then transferred from Dol-P through the action of oligosaccharyltransferase within the ER lumen to the appropriate Asn acceptor site on the nascent glycoprotein. Although much is known regarding the oligosaccharide conjugation reactions on both leaflets of the bilayer, relatively little is understood regarding the regulation of *cis*-IPTase activity and dolichol synthesis, a requisite process for all downstream reactions leading to glycosylation. *cis*-IPTase activity promotes the successive condensation of isopentenyl diphosphate (IPP) onto a FPP backbone, resulting in the generation of a long-chain polyprenyl diphosphate (Schenk *et al*, 2001a). This polyprenyl diphosphate is subsequently dephosphorylated by an unidentified phosphatase(s), generating a polyprenol. The α-isoprene unit of the

*Corresponding author. Department of Pharmacology and Vascular Biology and Therapeutics Program, Yale University School of Medicine, Amistad Research Building, VBT Program, 10 Amistad Street, New Haven, CT 06520, USA. Tel.: +1 203 737 2291; Fax: +1 203 737 2290; E-mail: william.sessa@yale.edu

Received: 20 December 2010; accepted: 13 April 2011; published online: 13 May 2011

polyprenol is then reduced by an NADPH-dependent microsomal reductase, resulting in the formation of dolichol.

The bacterial *cis*-IPTase, UPPS, catalyses the synthesis of the glycosyl carrier lipid undecaprenyl-PP, which is essential for peptidoglycan production (Kurokawa *et al*, 1971). The first identified eukaryotic *cis*-IPTase was cloned from *Saccharomyces cerevisiae* via an *rer* mutant strain (*rer2*) defective in ER protein sorting (Sato *et al*, 1999). Subsequently, a second *cis*-IPTase was cloned from yeast as a suppressor of *rer2*. This gene, *SRT1*, encodes a protein with significant sequence homology to RER2, yet is expressed differentially during the cell cycle and promotes the formation of a longer-chain dolichol than that produced by Rer2p (Sato *et al*, 2001; Schenk *et al*, 2001b). Sequence homology analysis resulted in the discovery of a human cDNA with similarity to bacterial and yeast *cis*-IPTases. This human *cis*-IPTase or hCIT (also referred to as HDS or DHDDS) complements growth and *cis*-IPTase defects in the *rer2* mutant strain. hCIT conforms to a reticular pattern of subcellular distribution by immunofluorescence, yet has no predicted transmembrane domains (Endo *et al*, 2003; Shridas *et al*, 2003). Furthermore, overexpression of hCIT in mammalian cells results in modest increases in *cis*-IPTase activity, suggesting the existence of accessory subunits of the *cis*-IPTase that may influence hCIT activity (Shridas *et al*, 2003).

In a screen for binding partners for the amino-terminus of reticulon 4B/Nogo-B, we discovered a binding protein we termed Nogo-B receptor (NgBR) (Miao *et al*, 2006). To elucidate potential intracellular roles of NgBR, we screened a cDNA expression library for proteins that interact with the C-terminus of NgBR and found that NgBR interacts with the cholesterol-binding protein Niemann-Pick type C2 (NPC2), a lysosomal protein that is essential for intracellular trafficking of LDL-derived cholesterol (Harrison *et al*, 2009). NgBR regulates NPC2 stability in the ER and the loss of NgBR reduces NPC2 protein levels and results in phenotypes reminiscent of NPC2 disease, including accumulation of free cholesterol and defects in cholesterol trafficking to the ER sterol sensing machinery.

Analysis of conserved domains in the NgBR sequence reveals a single domain with homology to *cis*-IPTases (Miao *et al*, 2006). Although *cis*-IPTase activity was described 40 years ago (Gough and Hemming, 1970), a paucity of information exists regarding the molecular components of this process. Upon examining the function of the conserved *cis*-IPTase domain in NgBR, we discovered a role for NgBR in modulating *cis*-IPTase activity and regulating dolichol biosynthesis in mammalian cells. These data provide new insights into the process of N-linked protein glycosylation and extend our understanding of the regulation of *cis*-IPTase activity and dolichol biosynthesis.

Results

The C-terminus of NgBR exhibits conformations consistent with NPC2 binding and regulation of N-linked glycosylation

Our previous work identified NgBR as an NPC2-binding protein that functions to promote NPC2 protein stability in the ER lumen. As part of our ongoing efforts to characterize the NgBR–NPC2 interaction, we discovered two conserved Asn residues in the human NgBR C-terminal domain (Figure 1A) that conform to the consensus motif for N-linked protein glycosylation (Asn-X-Ser/Thr). No other putative N-linked glycan acceptor sites conforming to the Asn-X-Ser/Thr consensus are found in NgBR. Asn-144 is found in mammals and fish, while Asn-271 is conserved in mammals (Figure 1A). Neither the Asn-144 nor the Asn-271 site is found in the yeast orthologue. Expression of wild-type (WT) human NgBR results in two distinct mobility shifts of

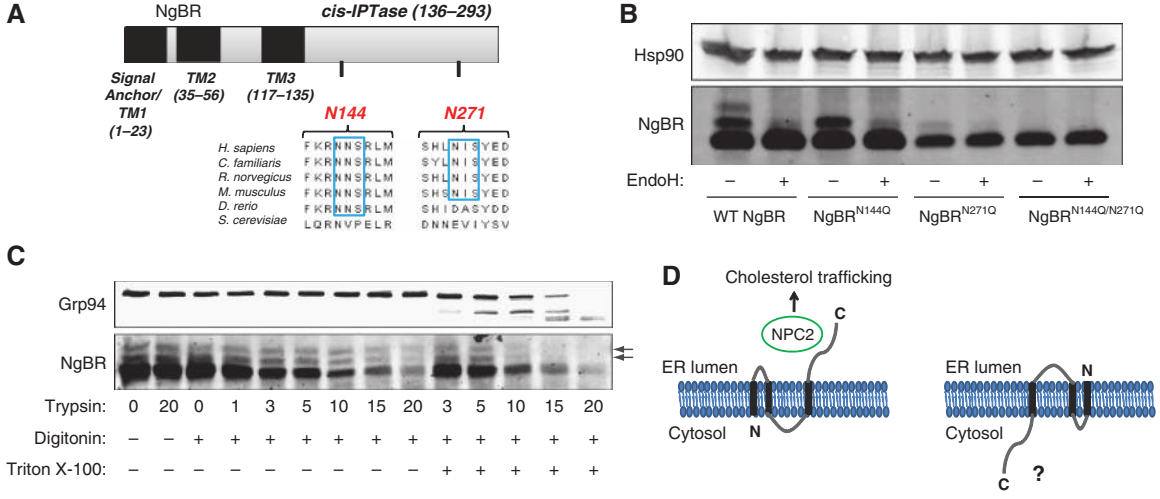

Figure 1 A major proportion of the NgBR C-terminus conforms to cytosolic orientation. (**A**) Primary structure of human NgBR. Two N-linked glycosylation sites are predicted (Asn-X-Ser) in the C-terminal domain of NgBR. Alignments were performed with ClustalW2. (**B**) COS-7 cells were transfected with NgBR constructs as indicated. At 24 h post-transfection, cell lysates were prepared and treated with Endoglycosidase H (EndoH). N144Q and N271Q mutants of NgBR result in differential EndoH sensitivity. NgBR was detected using anti-HA antibodies. (**C**) Limited proteolysis of NgBR. HeLa cells expressing NgBR were permeabilized with digitonin and/or Triton X-100 and treated with trypsin for the indicated times to assess protein topology. Arrows denote glycosylated NgBR species that are relatively resistant to digitonin-dependent trypsin digestion when compared with non-glycosylated NgBR. Grp94, an ER luminal chaperone, is used here as a control for permeabilization of the ER bilayer. NgBR was detected using anti-HA antibodies. (**D**) Model of NgBR topology in the ER bilayer. A minor proporation of NgBR exists with its C-terminus in a luminal orientation, where it interacts with NPC2 to promote intracellular cholesterol homeostasis. The major proportion of NgBR exists with its C-terminus in a cytosolic orientation with unknown function.

a fraction of the protein by SDS–PAGE. This fraction of NgBR is collapsed by digestion of high mannose-linked glycans with endoglycosidase H (EndoH) treatment (Figure 1B). The EndoH sensitivity of these bands provides evidence that a portion of the C-terminus of NgBR is glycosylated and present within the ER lumen. To further define the residues to which these glycans are linked, we mutated the putative glycosylation sites (Asn-144 and Asn-271 of hNgBR) to Gln. $NgBR^{N144Q}$ expression leads to loss of the uppermost band in the mobility shift, with the remaining portion exhibiting EndoH sensitivity (Figure 1B). Loss of glycosylation at Asn-271 ($NgBR^{N271Q}$) leads to a more dramatic loss of EndoH sensitivity, with an almost complete ablation of the shifted bands (Figure 1B). This more robust loss of glycosylation seen in the N271Q mutant may result from site selection by STT3 isoforms within the oligosaccharyltransferase complex, although this possibility awaits further analysis (Kelleher *et al*, 2003). Combined mutation of both glycosylation sites ($NgBR^{N144Q/N271Q}$) results in a complete loss of EndoH sensitivity (Figure 1B). Thus, a minor proportion of the NgBR C-terminus is glycosylated in an EndoH-sensitive manner, and therefore present in an orientation that is compatible with NPC2 binding in the lumen of the ER. It is also important to note that a large fraction of NgBR exists with its C-terminus oriented towards the cytosol as shown by limited proteolysis experiments. This topology is defined by trypsin sensitivity in digitonin-permeabilized cells (i.e. selective permeabilization of the plasma membrane). Immunoreactivity of the NgBR C-terminal HA epitope is reduced following digitonin treatment, whereas the ER luminal chaperone Grp94 remains resistant to trypsin unless intracellular membranes are permeabilized with Triton X-100 (Figure 1C). Importantly, the glycosylated NgBR species remain relatively resistant to trypsin in the presence of digitonin (Figure 1C), further suggesting that NgBR exists in at least two conformations, one in which the C-terminus is oriented within the ER lumen and another in which the C-terminus is oriented in the cytosol.

We have recently shown NgBR to contain a signal anchor motif at the extreme N-terminus of the protein (residues 1–23) (Harrison *et al*, 2009). The TMpred algorithm predicts the presence of two additional membrane-embedded regions (Figure 1A), between residues 35–56 ('TM2') and between residues 117–135 ('TM3'). The presence of the C-terminal glycosylation-dependent mobility shift seen with expression of WT NgBR provides an index by which to assess the topological orientation of the NgBR C-terminus. Expression of NgBR TM deletion constructs (deletion of TM1, TM2, or TM3) results in a striking change in NgBR mobility (Supplementary Figure S1A). Deletion of TM1 or TM3 leads to a complete loss of EndoH sensitivity, while deletion of TM2 has no effect. Thus, TM1 and TM3 may regulate an ER luminal orientation of the NgBR C-terminus. We used these NgBR TM deletion constructs as tools to further dissect the relative importance of a luminal NgBR C-terminus to an NgBR–NPC2 binding event. Whereas both WT NgBR and $NgBR^{\Delta TM2}$ co-immunoprecipitate with NPC2 (Supplementary Figure S1B), $NgBR^{\Delta TM1}$ and $NgBR^{\Delta TM3}$ do not interact with NPC2 (Supplementary Figure S1B). As the TM1 and TM3 deletions preclude a luminal orientation for the NgBR C-terminus, the absence of NPC2 binding by these constructs supports a role for a luminal NgBR C-terminus in the NgBR–NPC2 interaction. We cannot exclude the possibility that these glycan point mutations and TM deletions may result in protein misfolding. However, the differential EndoH sensitivity coupled with the functional analysis of NPC2 binding suggests that NgBR exists with two topological conformations, the minor fraction with its C-terminus oriented towards the lumen in an orientation that is consistent with the regulation of NPC2 stability (Harrison *et al*, 2009), and the major fraction oriented with its C-terminus directed towards the cytosol with an uncharacterized function(s) (Figure 1D). The remainder of this study seeks to define the function of this major fraction of NgBR.

The C-terminal 158 amino acids of NgBR exhibit 44% sequence similarity, with the ancestral *cis*-IPTase from *Micrococcus luteus*. Based on our analysis of NgBR topology, the predominant form of NgBR has its *cis*-IPTase domain oriented in the cytosol. As *cis*-IPTase activity is confined to the cytosolic leaflet of the ER bilayer and essential for dolichol production (Schenk *et al*, 2001a), we tested the contribution of NgBR to N-linked protein glycosylation. To determine the extent to which NgBR influences N-linked glycosylation, we used siRNA to diminish NgBR levels in an endothelial cell line, EA.hy926, in which we have previously shown NgBR-targeted RNAi to significantly reduce NgBR expression (Harrison *et al*, 2009). We incubated cells with a control siRNA or an NgBR siRNA, pulsed with [2-^{3}H]-mannose and analysed mannose incorporation into proteins by TCA precipitation and extensive washing of the pellets, followed by scintillation counting and fluorography. Tunicamycin (Tm) treatment was used as a positive control for inhibition of N-linked glycosylation. Knockdown of NgBR leads to a dramatic reduction in mannose incorporation into proteins (Figure 2A). This effect was not due to a loss of mannose uptake; indeed, NgBR RNAi caused a slight increase in cellular [^{3}H]-mannose uptake (Figure 2B). The loss of NgBR also reduces the levels of mannose-labelled proteins detected in the TCA-precipitated media as shown by fluorography (Figure 2C) and Tm treatment results in complete loss of mannose-labelled protein (Figure 2C). These data suggest that NgBR is necessary for N-linked glycosylation.

As an independent approach to define the relationship between NgBR and N-linked glycosylation, we used a non-radioactive method termed fluorophore-assisted carbohydrate electrophoresis (FACE) to measure endogenous levels of LLOs and their precursors at steady state (Gao and Lehrman, 2006). Although knockdown of NgBR in EA.hy cells did not cause any loss of UDP-GlcNAc, GDP-mannose, or UDP-Glc (data not shown), it did result in dramatic reduction in $Glc_3Man_9GlcNAc_2$-Dol (G3M9) levels (Figure 3A). Although loss of G3M9-LLO was consistently observed in a series of replicate RNAi experiments, we noted considerable variability in the amounts and types of truncated LLOs that accumulated (e.g. the species migrating between the G5 and G6 standards in Figure 3A was not detected in each experiment). Expression of an RNAi-resistant form of NgBR in cells treated with siRNA results in a rescue of G3M9 levels (Supplementary Figure S2A and B). Quantification of these LLO data confirms that loss of NgBR results in an approximate 75% reduction in mature G3M9 levels (Figure 3B). N-linked glycosylation of a single acceptor site requires one molecule of $Glc_3Man_9GlcNAc_2$-Dol, four molecules of Man-P-Dol, and three molecules of Glc-P-Dol (Schenk *et al*, 2001a). FACE analysis of monosaccharide-linked dolichols showed a

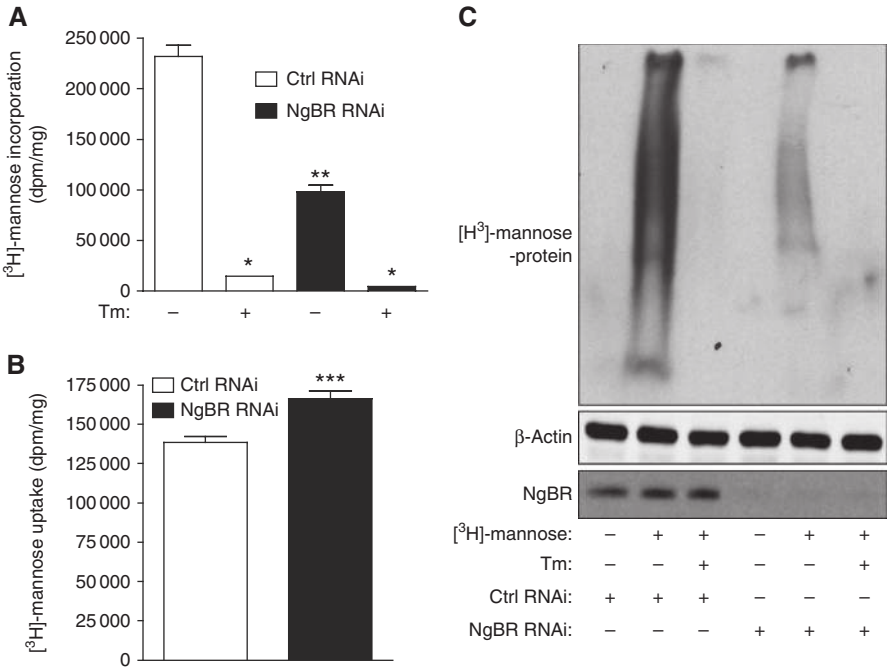

Figure 2 Loss of NgBR leads to diminished [^{3}H]-mannose-labelled proteins. (**A**) EA.hy926 cells were incubated with a control siRNA sequence (Ctrl RNAi) or an siRNA-targeting NgBR (NgBR RNAi) for 48 h before incubation with [^{3}H]-mannose. Following a 4-h incubation with [^{3}H]-mannose (during which uptake was linear), media was removed, cells were washed twice with PBS, lysed in RIPA buffer, and proteins were precipitated with 10% TCA. Precipitates were counted by scintillation or resolved by SDS–PAGE. Tunicamycin (Tm) treatment for 1 h before labelling was performed as a positive control for loss of [^{3}H]-mannose incorporation. (**B**) [^{3}H]-mannose uptake measurements were performed by subtracting scintillation counts in cell lysates from counts in extracellular media both pre- and post-incubation. (**C**) [^{3}H]-mannose-labelled, TCA-precipitated protein from cells treated with Ctrl RNAi or NgBR RNAi was resolved by SDS–PAGE and subjected to fluorography. An NgBR polyclonal antibody was used to detect endogenous NgBR expression whereas anti-β-actin was used to assess equal loading of the lysates (**A**, **B**, $n=3$; $^*P<0.001$, $^{**}P<0.001$, $^{***}P<0.001$).

significant reduction of these molecules as well (Figure 3C and D). These data are supported by analysis of total free glycan pools, which are also diminished after downregulation of NgBR expression (Supplementary Figure S2C–E). Taken together, results from mannose labelling and FACE experiments indicate that NgBR expression is necessary for efficient N-linked glycosylation and proper LLO biosynthesis. The presence of homology with enzymes that synthesize dolichol suggests that NgBR may influence glycosylation via effects on *cis*-IPTase activity.

NgBR is necessary for cis-IPTase activity and dolichol synthesis

Since loss of NgBR results in defects in LLO biosynthesis, we sought to determine whether NgBR influenced *cis*-IPTase activity. These activity measurements are performed using microsomal preparations in which radiolabelled IPP is incorporated into long-chain lipids using farnesyl diphosphate (FPP) as a starting substrate (Figure 4A) (Quellhorst *et al*, 1997). We prepared microsomes from cells expressing either endogenous NgBR or HA-tagged NgBR and performed western blots to ascertain the extent of NgBR expression in these membrane preparations. NgBR is found in membranes in both endogenous and overexpressed conditions (Supplementary Figure S3). Microsomal activity assays show that NgBR overexpression significantly enhances *cis*-IPTase activity (Figure 4B). In agreement with the mannose labelling and FACE analysis experiments, loss of NgBR expression results in a robust deficit in microsomal *cis*-IPTase activity (Figure 4C). Furthermore, this deficit in *cis*-IPTase activity is apparent over a wide range of initial substrate concentrations (Figure 4D). Separation analysis of these *cis*-IPTase reaction products by reverse phase thin layer chromatography (Figure 4E) indicates a loss of dolichol to undetectable levels following knockdown of NgBR. These data show that NgBR is necessary for *cis*-IPTase activity and dolichol biosynthesis.

We sought to define the mechanism by which NgBR regulates *cis*-IPTase activity. Five regions are conserved between the prokaryotic *cis*-IPTase UPPS and eukaryotic *cis*-IPTases from yeast (Rer2p and Srt1p) and human (hCIT) (Takahashi and Koyama, 2006). These regions are designated as being critical for catalysis and substrate binding as determined by structure/function analysis of the prokaryotic UPPS (Fujihashi *et al*, 2001; Kharel *et al*, 2001; Guo *et al*, 2005). Although the NgBR C-terminus exhibits 44% sequence similarity with the *M. luteus cis*-IPTase, phylogenetic comparison of NgBR with characterized *cis*-IPTases shows that NgBR and its yeast orthologue NUS1 cluster as a distinct subgroup of *cis*-IPTases (Figure 5A). Furthermore, sequence alignment (Supplementary Figure S4) of these *cis*-IPTases shows lack of many of the residues that have been defined as critical for catalysis and substrate binding through structural and functional studies of UPPS (Fujihashi *et al*, 2001; Kharel *et al*, 2001; Guo *et al*, 2005), suggesting that although NgBR and Nus1p have *cis*-IPTase homology domains, they may not be functional enzymes.

This partial homology with known *cis*-IPTases stimulates questions regarding the precise function of NgBR in regulating dolichol synthesis. The molecular components of eukaryotic *cis*-IPTase activity are relatively well described in

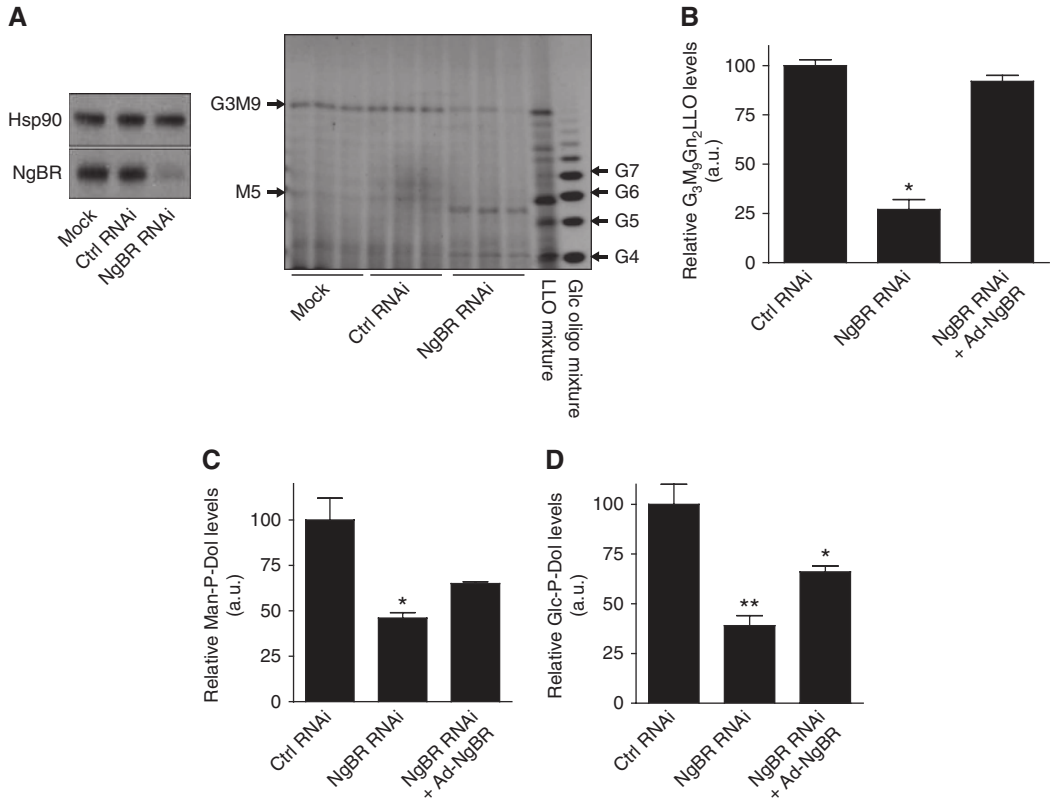

Figure 3 NgBR influences lipid-linked oligosaccharide (LLO) levels as measured by fluorophore-assisted carbohydrate electrophoresis (FACE). (**A**) SDS–PAGE of lysates from EA.hy cells treated with transfection reagent (mock), Ctrl RNAi, or NgBR RNAi. Right-hand panel shows LLO extracts from these cells that were subjected to FACE analysis as described in Materials and methods. 'G3M9' refers to the mature, ER luminal LLO G3M9Gn2-P-P-Dol, whereas 'M5' refers to the M5Gn2-P-P-Dol intermediate that flips from the cytoplasmic to the luminal leaflet of the ER lumen. 'LLO' refers to a standard mixture of dolichol-linked oligosaccharides, and 'glc oligo mixture' refers to a standard mixture of glucose polymers. Cells were treated with RNAi in for 48 h. (**B**) Quantification of G3M9 levels from FACE analysis. (**C**, **D**) Dolichol-linked monosaccharide analysis. Samples were extracted and FACE analysis was performed as described in Experimental Procedures. Quantification of Man-P-Dol (**C**) and Glc-P-Dol (**D**) levels from replicate FACE analyses (**C**, $n=9$, $^{*}P<0.0001$; **D**, $n=5$, $^{*}P<0.05$, $^{**}P<0.001^{*}$).

S. cerevisiae (Sato *et al*, 1999, 2001; Schenk *et al*, 2001b). In particular, the *rer2* strain that is deficient in dolichol synthesis is a useful tool to assess the contribution of a given gene to *cis*-IPTase activity. This strain exhibits temperature-sensitive growth defects, loss of N-linked glycosylation, deficiencies in GPI-anchored protein production, and aberrations in membrane morphology. The effects we observe in the preceding NgBR knockdown experiments reveal similarities with the *rer2* mutant strain, including loss of N-linked glycosylation and dolichol synthesis (Sato *et al*, 1999).

We transformed the *rer2* strain with constructs expressing the NgBR yeast orthologue NUS1 or with human NgBR to determine whether these putative *cis*-IPTases could rescue the growth and glycosylation-deficient phenotypes present in this strain. Neither NUS1 nor NgBR rescue the temperature-sensitive growth phenotype present in *rer2* (Figure 5B). Furthermore, expression of NUS1 and NgBR are not sufficient to rescue defects in carboxypeptidase Y (CPY) glycosylation seen in the *rer2* strain (Figure 5C). Analysis of *cis*-IPTase products by reverse phase TLC (Figure 5D) does not reveal any IPP-derived products generated by expression of either NUS1 or NgBR in the *rer2* null strain. Thus, NgBR is necessary but not sufficient for *cis*-IPTase activity and dolichol synthesis. Since NgBR does not share the same degree of conservation with UPPS as do the characterized eukaryotic *cis*-IPTases, we sought to determine if NgBR might somehow function as an obligate modifier of the previously characterized mammalian *cis*-IPTase and *RER2* orthologue, hCIT.

NgBR interacts with hCIT and facilitates cis-IPTase activity

As mentioned previously, *cis*-IPTase activity is associated with the cytosolic leaflet of the ER bilayer. Both NgBR and hCIT have been shown to localize primarily to the ER (Shridas *et al*, 2003; Harrison *et al*, 2009). We assessed the possibility that NgBR and hCIT might be associated in a protein complex, and performed co-immunoprecipitation experiments in HeLa cells expressing both proteins. Immunoprecipitation of hCIT-HA and the reciprocal immunoprecipitation of NgBR-FLAG reveal the presence of an interaction between these two proteins (Figure 6A and B). Furthermore, immunoprecipitation of hCIT-FLAG in CHO cells stably expressing a vector (as a control), full-length NgBR, or a C-terminal truncation mutant of NgBR lacking the *cis*-IPTase homology domain results in a co-immunoprecipitation with full-length NgBR only (Figure 6C), suggesting that the *cis*-IPTase domain of NgBR is necessary for its interaction with hCIT.

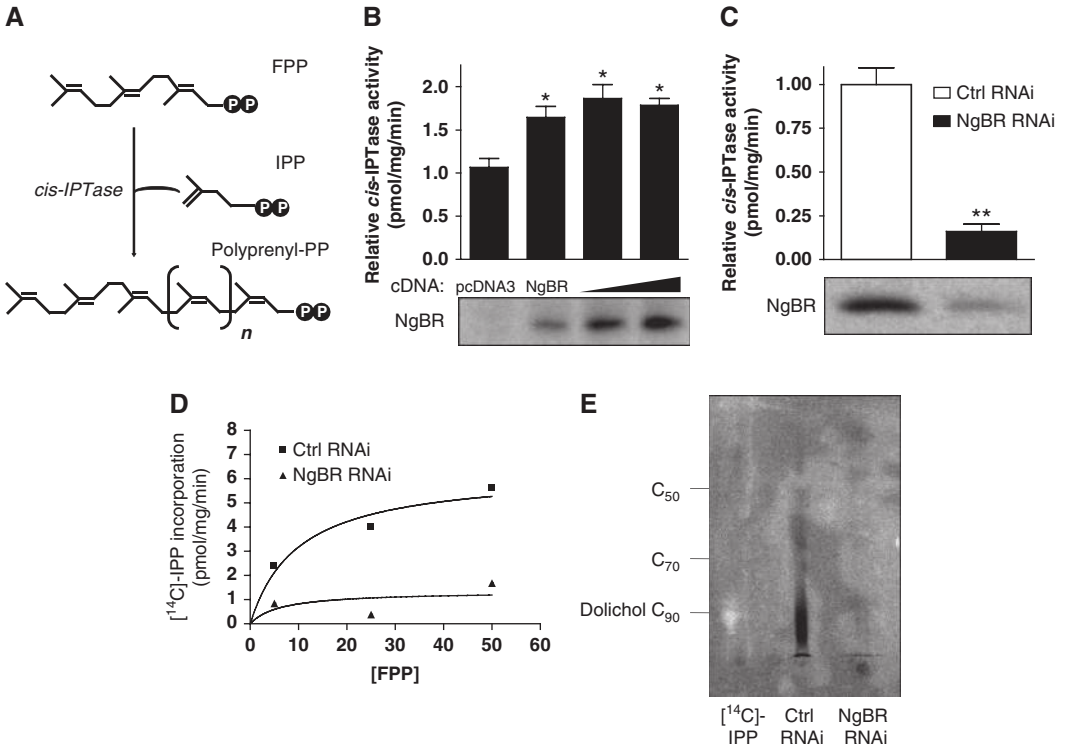

Figure 4 NgBR promotes *cis*-isoprenyltransferase activity. (**A**) *cis*-IPTase activity promotes the successive condensation of IPP using FPP as an initial substrate to generate a long-chain polyprenyl diphosphate. (**B**) *cis*-IPTase activity assays were performed as described in Materials and methods. CHO cells expressing control cDNA (pcDNA3) or increasing amounts of NgBR cDNA were fractionated and membranes incubated with radiolabelled IPP. (**C**) EA.hy926 cells were treated with Ctrl RNAi or NgBR RNAi for 48 h before fractionation. Reactions containing 25 mM Tris–HCl (pH 8.5), 5 mM $MgCl_2$, 1.25 mM DTT, 2.5 mM Na_3VO_4, 50 μM [^{14}C]-IPP, 100 μM FPP, and 100 μg of microsomal protein were incubated for 30 min at 37° for measurements of *cis*-IPTase activity. Reactions were stopped with 2 ml $CHCl_3$:MeOH (2:1). The organic phase was washed three times with $CHCl_3$:MeOH:dH_20 (3:48:47), dried under nitrogen, resuspended in hexane, and counted by scintillation. (**D**) Microsomal *cis*-IPTase assays were performed in EA.hy926 cells with varying concentrations of FPP as starting substrate. Results are the average duplicate measurements, and this experiment was repeated two additional times. (**E**) Reverse phase thin layer chromatography (TLC) of extracts from (**C**). Extracts were treated with potato acid phosphatase before sample loading (**B**, **C**, $n=3$, $n=4$, respectively; $^*P<0.01$, $^{**}P<0.005$).

We noticed a robust increase in NgBR protein levels when NgBR was co-expressed with hCIT (Figure 6A). In order to determine the functional consequences of the NgBR–hCIT interaction, we co-expressed both proteins, either holding the concentration of hCIT constant with increasing concentrations of NgBR cDNA (Figure 7A), or holding the concentration of NgBR constant with increasing concentrations of hCIT (Figure 7B). In both cases, co-expression of NgBR and hCIT results in enhanced levels of its binding partner, providing evidence of a stabilizing effect between these two proteins. This interaction also brought forth the possibility that NgBR might serve as a docking site for hCIT on the ER membrane, since hCIT localizes to the ER, yet has no predicted transmembrane domain by hydropathy analysis (Shridas *et al*, 2003). In order to address whether NgBR functions as an ER-binding site for hCIT, we reduced NgBR levels using shRNAs in HeLa cells. Although total levels of hCIT were lower in cells with knockdown of NgBR (consistent with a promotion of hCIT stability in the presence of the NgBR interaction), the relative amount of hCIT associated with the membrane fraction remains unchanged (Figure 7C). These data suggest that targeting of hCIT to the ER is likely independent of its interaction with NgBR.

Of note, expression of hCIT in the *rer2* background rescues neither growth nor CPY glycosylation to the same extent as does expression of RER2 (Figure 5B–D). In light of the interaction between NgBR and hCIT and the effects of NgBR on hCIT protein levels, we tested the hypothesis that NgBR might potentiate the *cis*-IPTase activity of hCIT. Expression of hCIT in the *rer2* strain results in a modest rescue of dolichol levels with increased lipid chain length (>C90; Figure 7D). Co-expression of NgBR with hCIT leads to a striking potentiation of long-chain dolichol synthesis (Figure 7D). Collectively, these data provide evidence of a new mode of *cis*-IPTase regulation and dolichol production via the hCIT-binding protein NgBR (Figure 7E).

Discussion

Dolichol is an obligate carrier of glycans for N-linked protein glycosylation, protein O-mannosylation, C-mannosylation, and GPI anchor biosynthesis. We have found that NgBR is necessary for N-linked protein glycosylation, production of mature LLOs, microsomal *cis*-IPTase activity and dolichol synthesis. Furthermore, NgBR interacts with and stabilizes the *cis*-IPTase, hCIT. Given the relatively weak enzymatic activity associated with hCIT in mammalian *cis*-IPTase assays coupled with the lack of complete rescue of the dolichol-deficient *rer2* mutant strain with hCIT, we propose that NgBR functions as an allosteric regulator or accessory protein in a *cis*-IPTase complex through its interaction with hCIT. This idea is supported by the stabilizing effect of NgBR on hCIT

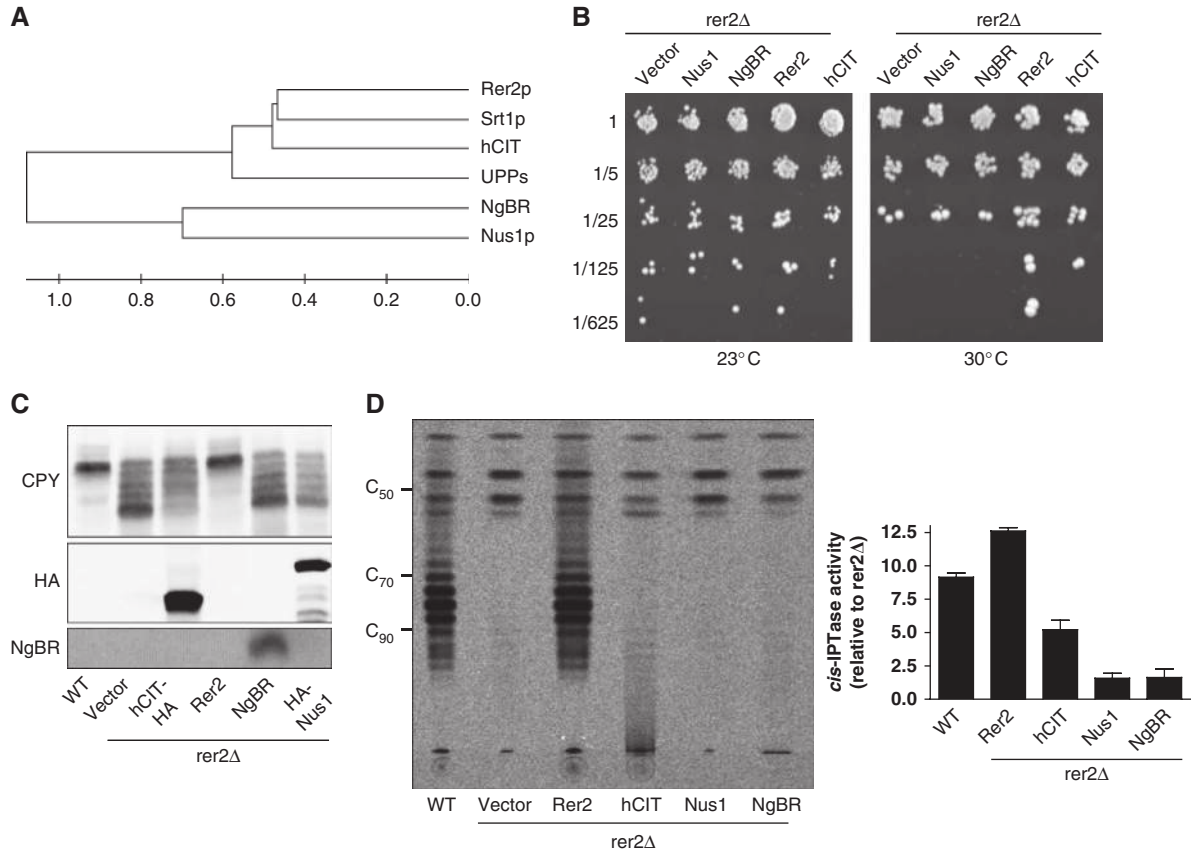

Figure 5 NgBR and its yeast orthologue are divergent from characterized *cis*-IPTases. (**A**) Phylogenetic analysis of *cis*-IPTases: *M. luteus*, O82827 (UPPS); *S. cerevisiae*, NP_013819 (Srt1p), NP_009556 (Rer2p), NP_079162 (hCIT), NP_612468 (NgBR), NP_010088 (Nus1p). The tree was constructed using MEGA (version 4.0). Divergence (arbitrary units) is designated in the lower scale. (**B**) *rer2* strains expressing the indicated constructs were grown at either room temperature or 30°. (**C**) SDS–PAGE of protein extracts assessing carboxypeptidase Y (CPY) glycosylation from WT (SS328) and *rer2* strains expressing the indicated constructs. (**D**) Reverse phase TLC separation of microsomal *cis*-IPTase extracts from the indicated strains. Densitometric results from triplicate measurements of *cis*-IPTase reaction products are quantified in the right panel as a relative measurement of products from *rer2*.

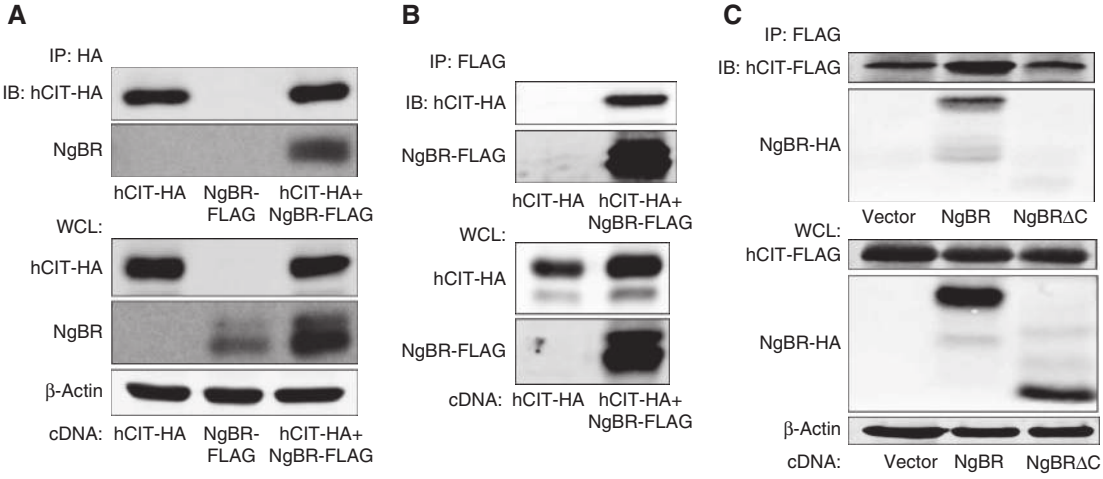

Figure 6 NgBR interacts with hCIT. (**A**) HeLa cells were co-transfected with hCIT-HA and NgBR-FLAG. At 24 h post-transfection, cells were lysed and lysates were incubated with anti-HA antibodies. Immunoprecipitates were resuspended in 2 × SDS before resolution by SDS–PAGE. (**B**) Reciprocal immunoprecipitations were performed with NgBR-FLAG and hCIT-HA by incubating lysates with anti-FLAG antibodies. (**C**) CHO cells stably expressing empty vector (Vector), full-length, HA-tagged NgBR (NgBR), or a truncated HA-tagged mutant of NgBR lacking the C-terminus (NgBRΔC) were transfected with hCIT-FLAG. At 24 h post-transfection, cells were lysed and hCIT-FLAG was immunoprecipitated. IP, immunoprecipitate; WCL, whole-cell lysate.

protein levels, the NgBR-dependent potentiation of *cis*-IPTase activity and the marked reduction in glycosylated proteins, LLOs and *cis*-IPTase activity after NgBR knockdown. NgBR is not sufficient to rescue the *rer2* mutant strain, arguing against it being an independent, single-subunit enzyme; however, NgBR potentiates dolichol production in an hCIT-dependent

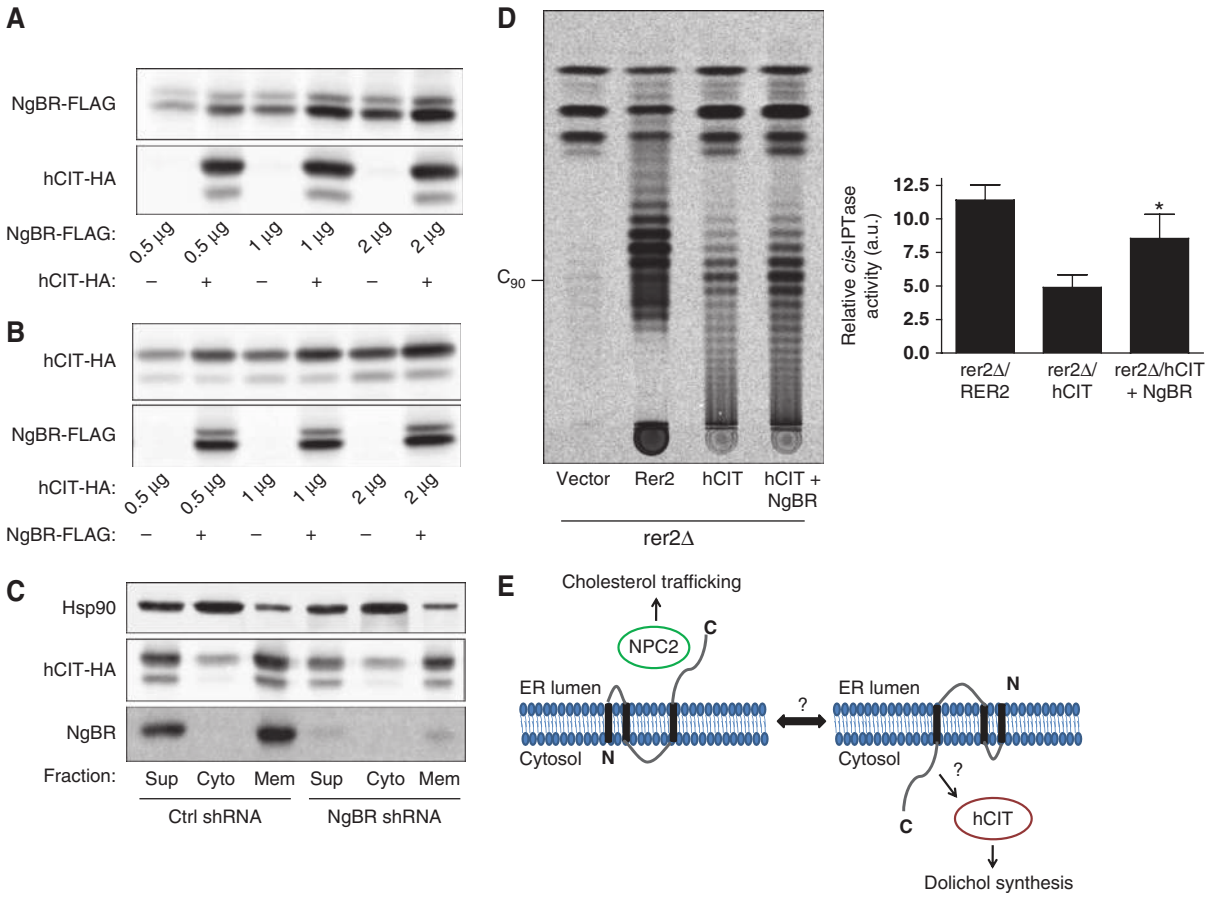

Figure 7 NgBR stabilizes hCIT protein levels and potentiates hCIT-mediated *cis*-IPTase activity in yeast. (**A**, **B**) HeLa cells were transfected with either hCIT-HA or NgBR-FLAG cDNA at a constant 2 μg and the opposing cDNA (e.g. hCIT-HA versus NgBR-FLAG) co-transfected at the scaled amounts are shown. Cells were lysed 24 h post-transfection and lysates were resolved by SDS–PAGE. (**C**) HeLa cells stably infected with lentivirus expressing a control short hairpin RNA (Ctrl shRNA) or an shRNA directed against NgBR (NgBR shRNA) were transiently transfected with hCIT. At 24 h post-transfection, membranes were prepared at 10^5 *g* and the indicated proteins were detected by western blotting. Sup, post-nuclear supernatant; Cyto, cytosolic fraction; Mem, membrane fraction. (**D**) Reverse phase TLC separation of microsomal *cis*-IPTase extracts from *rer2* strains expressing hCIT or hCIT + NgBR. Densitometric results from triplicate measurements of *cis*-IPTase reaction products are quantified in the right panel as a relative measurement of products from *rer2* ($^*P<0.05$, $n=3$). (**E**) Model of NgBR topology in the ER bilayer. The major proportion of NgBR exists with its C-terminus in a cytosolic orientation where NgBR may bind hCIT directly (in a manner that is dependent on the NgBR C-terminus) or through as yet unidentified accessory proteins and thereby regulates dolichol biosynthesis. The possibility of dynamic interplay between the two conformations of NgBR (C-term$_{luminal}$ or C-term$_{cytosolic}$) is depicted by a dual arrow between the topologies.

manner. Collectively, these findings advance our understanding of dolichol biosynthesis.

The C-terminal region of NgBR is conserved and sequence homology to NgBR exists in *S. cerevisiae*, *Drosophila melanogaster*, *Arabidopsis thaliana*, and *Mus musculus*. Interestingly, the yeast orthologue of NgBR, *NUS1* (*YDL193w*) is an essential gene and was identified in a screen for genes that influence cell-cycle progression (Yu *et al*, 2006). Loss of *NUS1* was found to disrupt glycosylation of CPY, secretion of alkaline phosphatase, and production of the GPI-linked protein Gas1p. These data further support a role for NgBR in N-linked glycosylation and *cis*-IPTase activity. It is of interest to determine whether NgBR is a functional orthologue of *NUS1* as an extension of these findings. Analysis of the relationship between *NUS1* and the hCIT orthologue *RER2* may provide meaningful insights into the regulation of *cis*-IPTase activity. Single deletions of each yeast *cis*-IPTase *RER2* or *SRT1* results in growth defects, yet the cells remain viable (Sato *et al*, 1999, 2001; Schenk *et al*, 2001b). Loss of *NUS1*, however, leads to lethality (Yu *et al*, 2006). This is somewhat surprising, given the greater degree of homology between *RER2*, *SRT1*, and the ancestral *cis*-IPTase UPPS. We favour the hypothesis that *NUS1* may function upstream of both yeast *cis*-IPTases, although this possibility awaits further study.

Previously, we have shown that NgBR regulates NPC2 stability and thereby promotes trafficking of LDL-derived cholesterol (Harrison *et al*, 2009). Here, we show that TM1 and TM3 of NgBR are critical for its interaction with NPC2. Since glycosylated NgBR represents <20% of the total protein, we proposed that NgBR exerts an additional function on the cytosolic face of the ER. Our data clearly show that the predominant form of NgBR exists in an EndoH-resistant state, demonstrating that NgBR likely exists in alternate topological conformations. Alternate membrane topologies have been described for a number of other proteins. Large-scale topology reporter screens conducted in *Escherichia coli* and *S. cerevisiae* identified a subset of proteins with alternate (cytosolic versus luminal) C-terminal orientations (Daley *et al*, 2005; Kim *et al*, 2006). The prevailing model posits a

thermodynamic driving force for transmembrane helix insertion, implying that weakly inserting helices may result in proteins with alternate topologies as a function of the relative hydrophobicity of the helix (Hessa *et al*, 2005, 2007). Our data suggest that the C-terminus of NgBR exists in two topological orientations: a minor glycosylated species in the lumen of the ER where it interacts with NPC2, and a predominant species in the cytosol where it regulates *cis*-IPTase activity and binds hCIT. The precise mechanism by which these topologies are regulated awaits further detailed analysis.

Although our results clearly show that NgBR is necessary for hCIT function, a number of interesting questions remain. The vast proportion (~80–90%) of cellular dolichol is present as an esterified lipid or free alcohol, and is therefore in a chemical form not compatible with a glycan carrier lipid function. Whether this large pool of dolichol functions as a reservoir to be phosphorylated and used as a glycan carrier is unknown. No functions have been ascribed to these non-phophorylated dolichol species, though some evidence suggests that dolichol disrupts bilayers and increases membrane fluidity (Lamson *et al*, 1994; Zhou and Troy, 2005; Wang *et al*, 2008). Identification of NgBR as a necessary component of the dolichol biosynthesis machinery brings us a step closer towards a more complete understanding of the roles of this essential polyisoprene lipid.

Materials and methods

Materials

D-[2-^{3}H]-mannose (15–30 Ci/mmol) was purchased from Perkin-Elmer. Express [^{35}S] protein labelling mix (NEG-072) was also purchased from Perkin-Elmer. [1-^{14}C]-IPP (50 mCi/mmol) was purchased from Sigma. Tm was purchased from EMD Biosciences; FPP, orthovanadate, and DTT were purchased from Sigma. Normal phase TLC plates were purchased from EMD Biosciences; RP-TLC plates were from Whatman. Dolichol standards (C_{50}–C_{70} and C_{90}) were purchased from Indofine Chemical Co. Antibodies used in this study include α-myc (Cell Signaling), α-HA (Roche), β-actin (Sigma), α-NgBR (Imgenex), α-FLAG (Sigma), Hsp90 (BD Biosciences), Calnexin (E10, Santa Cruz), CPY (Invitrogen), HA affinity matrix (Sigma), FLAG agarose (Sigma), NPC2 (H-125, Santa Cruz), Nogo-B (N-18, Santa Cruz). Constructs used in this study include NgBR-HA was cloned into pcDNA3 using *Hin*dIII and *Eco*RI; hCIT-HA was cloned into pcDNA3 using *Kpn*I and *Xba*I; hCIT-FLAG was cloned into pIRES using *Not*I and *Eco*RI; hCIT was cloned into p426-GPD and p423-GPD using *Spe*I and *Sal*I; NgBR and *Nus*1 were cloned into p426-GPD or p423-GPD with *Bam*HI and *Sal*I.

Limited proteolysis

HeLa cells expressing NgBR were scraped into KHM buffer (110 mM KAc, 20 mM HEPES, 2 mM $MgCl_2$). In all, 50 μM digitonin was added to the KHM buffer for 5 min at room temperature in some tubes to selectively permeabilize the plasma membrane. Following digitonin permeabilization, cells were washed once with KHM buffer. Trypsin (1.12 U/ml; Roche) was added to cells in KHM buffer for the indicated times in the presence or absence of 1% Triton X-100. Reactions were stopped by addition of 400 U soybean trypsin inhibitor (Sigma), then prepared for immunoblotting. Antibodies used for immunoblotting were anti-HA (Roche) 1:1000 and anti-GRP94 (Assay Design, 9G10). Arrows denote glycosylated NgBR species that are relatively resistant to digitonin-dependent trypsin digestion when compared with non-glycosylated NgBR.

[2-^{3}H]-mannose incorporation

EA.hy926 cells were grown in 60 mm dishes until ~80–90% confluent. Growth medium was then removed and replaced with glucose-free DMEM supplemented with 0.1 mg/ml glucose and 5% dialyzed FCS. Cells were incubated in reduced glucose medium for 1 h. Some plates received Tm (5 μg/ml) as a control for inhibition of N-linked glycosylation during the 1-h incubation period. After 1 h, 20 μCi/ml [2-^{3}H]-mannose was added to each plate and cells were incubated at 37° for 4 h. Following the incubation period, cells were washed twice with PBS, lysed in RIPA buffer, and aliquots of both conditioned media and lysates were collected for determination of mannose uptake values. Cell lysates or conditioned media were then subjected to precipitation of proteins with 10% TCA for 1 h on ice. Precipitates were washed four times with 10% TCA, resuspended in 6 M Urea/SDS buffer, and boiled until pellets were in solution (~30 min). TCA precipitates were counted by scintillation or resolved by SDS–PAGE. Gels were fixed, incubated with ENHANCE reagent, and then dried for 1 h at 80° before exposure to film at −80° for 1 week.

Fluorophore-assisted carbohydrate electrophoresis (FACE) analysis

Detection of LLOs, lipid-linked monosaccharides, and nucleotide sugars was performed essentially as described (Gao and Lehrman, 2006). Analysis of free glycans was performed by treating total protein precipitates with *N*-glycanase and separating neutral and acidic glycans by ion exchange chromatography, followed by FACE analysis of the free glycans. Each condition was prepared initially from a 15-cm plate of confluent EA.hy cells in normal growth medium, and scraped into a methanolic suspension and processed according to the established procedures.

Microsomal cis-IPTase activity

Cells were cultured in 15 cm dishes until reaching 100% confluency. For each condition, three 15 cm dishes were pooled for preparation of crude microsomes. Cells were scraped into PBS containing 1 mM EDTA, collected with a 500-*g* spin, and resuspended in hypotonic buffer (10 mM HEPES, pH 7.9, 1.5 mM $MgCl_2$, 10 mM KCl, 250 mM sucrose). Cells were incubated in hypotonic buffer on ice for 10 min, followed by homogenization using a tight-fitting dounce homogenizer on ice. Unbroken material was cleared with a 1000-*g* centrifugation, and the supernatant from this spin was re-centrifuged at 100 000 *g* for 35 min at 4°. Post-100 000 *g* pellets were washed twice with *cis*-IPTase reaction buffer (25 mM Tris–HCl, pH 7.4, 5 mM $MgCl_2$, 1.25 mM DTT, 2.5 mM sodium orthovanadate), then resuspended in reaction buffer. Reaction mixtures from mammalian cells contained 100 μg microsomal protein, 25 μM FPP, 50 μM [1-^{14}C]-isopentenyl pyrophosphate (IPP) (55 mCi/mmol), and 0.35% Triton X-100 in a total volume of 0.1 ml. For *cis*-IPTase experiments using microsomes from yeast, post-100 000 *g* pellets were washed twice and then resuspended in yeast *cis*-IPTase reaction buffer (60 mM HEPES, pH 8.5, 5 mM $MgCl_2$, 2 mM DTT, 2 mM NaF, 2 mM sodium orthovanadate). Yeast reaction mixtures contained 100 μg microsomal protein, 50 μM FPP, and 45 μM IPP. Reactions were incubated at 37° for 1 h and quenched by addition of 2 ml $CHCl_3$:MeOH (2:1). Products were separated from unreacted water-soluble IPP by partition through addition of 0.8 ml of 0.9% NaCl. The organic phase was washed three times with $CHCl_3$:MeOH:dH_2O (3:48:47) and dried under nitrogen. For normal phase thin layer chromatography, samples were resuspended in 50 μl *n*-hexane, and aliquots were counted by scintillation. The remainder of the sample was loaded onto an activated silica gel 60 TLC plate (EMD, 20 × 20 cm^2, #5721-7) and run in a hexane:ethyl acetate (80:20) buffer. The relative size of the products was measured according to the addition of standards to each lane that were visualized with iodine vapour. After drying, the plate was exposed to a phosphor screen for 2 weeks and imaged using a Typhoon phosphorimager. For analysis of products using reverse phase TLC, samples were prepared according to Fujii *et al* (1982). Samples were resuspended in 1 ml of 1-butanol after washing and drying under nitrogen. The butanol was transferred to an 8-ml screw-top glass vial to which 120 μl of 2.5 M sodium acetate, pH 4.7 was added, followed by addition of 3 ml of MeOH. At this point, 77 μl of 10% Triton X-100 was added to the vials, and each mixture was vortexed vigorously. In all, 16 U of potato acid phosphatase (dissolved in 250 mM sodium acetate buffer) was added to each reaction in order to dephosphorylate the polyprenyl-PP products. The reactions were incubated overnight at 37°, and 100 μl of 6 M NaOH was added to terminate the reaction. Dephosphorylated lipids were extracted three times with 2 ml *n*-hexane, extracts were pooled and washed two times with 2 ml dH_20. After the organic phase was dried under nitrogen, products were redissolved in 50 μl

n-hexane and from which an aliquot was subjected to scintillation counting. The remainder of the lipid was loaded onto a Whatman Partisil LKC18 RP-TLC plate ($20 \times 20\,cm^2$, #4800-800) in a mobile phase of acetone:dH_20 (95:2.5). Plates were dried at RT followed by heating at 80° for 5 min. Standards were visualized by exposure to iodine vapour and plates were exposed to a phosphor screen for 1–3 weeks; radiolabelled products were detected by phosphorimaging.

Immunoprecipitation and western blot analysis

For immunoprecipitation, cells were scraped and lysed in IP buffer. (IP buffer: 50 mM HEPES, 150 mM NaCl, 1 mM EDTA, 1% Triton X-100, 1.5 mg/ml protease inhibitor cocktail, 0.25 mg/ml AEBSF). Cells were homogenized using a loose-fitting dounce homogenizer. Lysates were cleared at 14 000 r.p.m. and 50 µl of anti-HA affinity matrix (Roche), or FLAG agarose (Sigma) were used to pulldown the HA-tagged protein or FLAG-tagged protein, respectively, from 2 mg of cell lysate. Following incubation at 4° for 2 h, the antibody-agarose conjugates were washed three times with IP buffer, resuspended in 2 × SDS loading buffer and boiled for 5 min before western blotting. For western blot analysis from whole-cell lysates, cells were lysed in a modified RIPA buffer (RIPA buffer: 50 mM Tris–HCl pH 7.4, 0.1% SDS, 0.1% sodium deoxycholate, 0.1 mM EDTA, 0.1 mM EGTA, 1% NP-40, 1.5 mg/ml protease inhibitor cocktail, 0.25 mg/ml AEBSF).

Yeast strains and culture conditions

S. cerevisiae strains used in these studies include SS328 (WT) is MATα ade2-101 ura3-52 his3Δ200 lys2-801 and rer2 YG932 is MATα Δrer2::kanMX4 ade2-101 ura3-52 his3Δ200 lys-801. Cultures were grown at 30° in YPD, Ura-selective YNB (6.7 g/l), or Ura-, His-selective YNB. Lysates were prepared from yeast by resuspension of cultures ($OD_{600} = 0.4–0.6$) in 100 µl/7.5 OD_{600}U of lysis buffer (50 mM Tris–HCl, pH 6.8, 150 mM NaCl, 1 mM EDTA, 0.1% NP-40, 1.5 mg/ml protease inhibitor cocktail (Roche), 0.25 mg/ml AEBSF (Roche)), plus an equal volume of 500 µm glass beads. Lysates were vortexed vigorously for 15 min at 4° in order to disrupt cell walls. Beads were collected by centrifugation at 2000 r.p.m. for 5 min at 4° followed by re-centrifugation of the lysates at 14 000 r.p.m. for 10 min to clear insoluble material. The supernatants were collected and stored at −20° before resolution by SDS–PAGE.

Statistical analyses

Data are expressed as mean ± s.e. Statistical comparisons between groups were performed using Student's *t*-test or analysis of variance using Graphpad Software. Significant differences are indicated in the figures.

Supplementary data

Supplementary data are available at *The EMBO Journal* Online (http://www.embojournal.org).

Acknowledgements

This work was supported by Grants R01 HL64793, R01 HL61371, R01 HL081190, RO1 HL096670, and P01 HL70295 from the National Institutes of Health to WCS; R01 GM38545 from the National Institutes of Health and I-1168 from the Welch Foundation to MAL; R01 GM36065 from the National Institutes of Health to CJW; and by a Pre-Doctoral Fellowship from the American Heart Association to KDH.

Author contribution: The overall study was conceived and designed by KDH and WCS, with important contributions from CJW, MAL, and JSR. KDH, AK, EJP, and NG performed the experiments and analysed the data. KDH and WCS wrote the paper, with contributions from MAL and CJW.

Conflict of interest

The authors declare that they have no conflict of interest.

References

Adair Jr WL, Cafmeyer N, Keller RK (1984) Solubilization and characterization of the long chain prenyltransferase involved in dolichyl phosphate biosynthesis. *J Biol Chem* **259:** 4441–4446

Burda P, Aebi M (1999) The dolichol pathway of N-linked glycosylation. *Biochim Biophys Acta* **1426:** 239–257

Daley DO, Rapp M, Granseth E, Melen K, Drew D, von Heijne G (2005) Global topology analysis of the Escherichia coli inner membrane proteome. *Science* **308:** 1321–1323

Endo S, Zhang YW, Takahashi S, Koyama T (2003) Identification of human dehydrodolichyl diphosphate synthase gene. *Biochim Biophys Acta* **1625:** 291–295

Fujihashi M, Zhang YW, Higuchi Y, Li XY, Koyama T, Miki K (2001) Crystal structure of cis-prenyl chain elongating enzyme, undecaprenyl diphosphate synthase. *Proc Natl Acad Sci USA* **98:** 4337–4342

Fujii H, Koyama T, Ogura K (1982) Efficient enzymatic hydrolysis of polyprenyl pyrophosphates. *Biochim Biophys Acta* **712:** 716–718

Gao N, Lehrman MA (2006) Non-radioactive analysis of lipid-linked oligosaccharide compositions by fluorophore-assisted carbohydrate electrophoresis. *Methods Enzymol* **415:** 3–20

Gough DP, Hemming FW (1970) The characterization and stereochemistry of biosynthesis of dolichols in rat liver. *Biochem J* **118:** 163–166

Grunler J, Ericsson J, Dallner G (1994) Branch-point reactions in the biosynthesis of cholesterol, dolichol, ubiquinone and prenylated proteins. *Biochim Biophys Acta* **1212:** 259–277

Guo RT, Ko TP, Chen AP, Kuo CJ, Wang AH, Liang PH (2005) Crystal structures of undecaprenyl pyrophosphate synthase in complex with magnesium, isopentenyl pyrophosphate, and farnesyl thiopyrophosphate: roles of the metal ion and conserved residues in catalysis. *J Biol Chem* **280:** 20762–20774

Harrison KD, Miao RQ, Fernandez-Hernando C, Suarez Y, Davalos A, Sessa WC (2009) Nogo-B receptor stabilizes Niemann-Pick type C2 protein and regulates intracellular cholesterol trafficking. *Cell Metab* **10:** 208–218

Hessa T, Kim H, Bihlmaier K, Lundin C, Boekel J, Andersson H, Nilsson I, White SH, von Heijne G (2005) Recognition of transmembrane helices by the endoplasmic reticulum translocon. *Nature* **433:** 377–381

Hessa T, Meindl-Beinker NM, Bernsel A, Kim H, Sato Y, Lerch-Bader M, Nilsson I, White SH, von Heijne G (2007) Molecular code for transmembrane-helix recognition by the Sec61 translocon. *Nature* **450:** 1026–1030

Kelleher DJ, Karaoglu D, Mandon EC, Gilmore R (2003) Oligosaccharyltransferase isoforms that contain different catalytic STT3 subunits have distinct enzymatic properties. *Mol Cell* **12:** 101–111

Kharel Y, Zhang YW, Fujihashi M, Miki K, Koyama T (2001) Identification of Significant residues for homoallylic substrate binding of Micrococcus luteus B-P 26 undecaprenyl diphosphate synthase. *J Biol Chem* **276:** 28459–28464

Kim H, Melen K, Osterberg M, von Heijne G (2006) A global topology map of the Saccharomyces cerevisiae membrane proteome. *Proc Natl Acad Sci USA* **103:** 11142–11147

Kurokawa T, Ogura K, Seto S (1971) Formation of polyprenyl phosphates by a cell-free enzyme of Micrococcus lysodeikticus. *Biochem Biophys Res Commun* **45:** 251–257

Lamson MJ, Herbette LG, Peters KR, Carson JH, Morgan F, Chester DC, Kramer PA (1994) Effects of hexagonal phase induction by dolichol on phospholipid membrane permeability and morphology. *Int J Pharm* **105:** 259–272

Miao RQ, Gao Y, Harrison KD, Prendergast J, Acevedo LM, Yu J, Hu F, Strittmatter SM, Sessa WC (2006) Identification of a receptor necessary for Nogo-B stimulated chemotaxis and morphogenesis of endothelial cells. *Proc Natl Acad Sci USA* **103:** 10997–11002

Quellhorst Jr GJ, Hall CW, Robbins AR, Krag SS (1997) Synthesis of dolichol in a polyprenol reductase mutant is restored by elevation of cis-prenyl transferase activity. *Arch Biochem Biophys* **343:** 19–26

Rip JW, Rupar CA, Ravi K, Carroll KK (1985) Distribution, metabolism and function of dolichol and polyprenols. *Prog Lipid Res* **24:** 269–309

Sato M, Fujisaki S, Sato K, Nishimura Y, Nakano A (2001) Yeast Saccharomyces cerevisiae has two cis-prenyltransferases with

different properties and localizations. Implication for their distinct physiological roles in dolichol synthesis. *Genes Cells* **6:** 495–506

Sato M, Sato K, Nishikawa S, Hirata A, Kato J, Nakano A (1999) The yeast RER2 gene, identified by endoplasmic reticulum protein localization mutations, encodes cis-prenyltransferase, a key enzyme in dolichol synthesis. *Mol Cell Biol* **19:** 471–483

Schenk B, Fernandez F, Waechter CJ (2001a) The ins(ide) and out(side) of dolichyl phosphate biosynthesis and recycling in the endoplasmic reticulum. *Glycobiology* **11:** 61R–70R

Schenk B, Rush JS, Waechter CJ, Aebi M (2001b) An alternative cis-isoprenyltransferase activity in yeast that produces polyisoprenols with chain lengths similar to mammalian dolichols. *Glycobiology* **11:** 89–98

Schroepfer Jr GJ (1981) Sterol biosynthesis. *Annu Rev Biochem* **50:** 585–621

Schroepfer Jr GJ (1982) Sterol biosynthesis. *Annu Rev Biochem* **51:** 555–585

Shridas P, Rush JS, Waechter CJ (2003) Identification and characterization of a cDNA encoding a long-chain cis-isoprenyltranferase involved in dolichyl monophosphate biosynthesis in the ER of brain cells. *Biochem Biophys Res Commun* **312:** 1349–1356

Swiezewska E, Danikiewicz W (2005) Polyisoprenoids: structure, biosynthesis and function. *Prog Lipid Res* **44:** 235–258

Takahashi S, Koyama T (2006) Structure and function of cis-prenyl chain elongating enzymes. *Chem Rec* **6:** 194–205

Teclebrhan H, Olsson J, Swiezewska E, Dallner G (1993) Biosynthesis of the side chain of ubiquinone:trans-prenyltransferase in rat liver microsomes. *J Biol Chem* **268:** 23081–23086

Wang X, Mansourian AR, Quinn PJ (2008) The effect of dolichol on the structure and phase behaviour of phospholipid model membranes. *Mol Membr Biol* **25:** 547–556

Yu L, Pena Castillo L, Mnaimneh S, Hughes TR, Brown GW (2006) A survey of essential gene function in the yeast cell division cycle. *Mol Biol Cell* **17:** 4736–4747

Zhou GP, Troy II FA (2005) NMR studies on how the binding complex of polyisoprenol recognition sequence peptides and polyisoprenols can modulate membrane structure. *Curr Protein Pept Sci* **6:** 399–411

